

### **3.1.3 Fischer-Tropsch Synthesis. Compositional Changes in an Iron Catalyst During Activation And Use**

#### **ABSTRACT**

The equilibrium phase compositions of iron have been calculated for gas compositions that could be encountered during the Fischer-Tropsch synthesis. The gas compositions measured experimentally for CO conversion levels in the 30-90% range show that iron should be present as the carbide phase. However, experimental characterization of iron catalysts show that a significant fraction of the iron is present as  $\text{Fe}_3\text{O}_4$  following synthesis for several days. A model that can account for the experimental catalyst phase composition and the gases present in the reactor would have a core of  $\text{Fe}_3\text{O}_4$  and an outer layer of iron carbides.

#### **INTRODUCTION**

The CHO system is of great importance in many areas of modern technology, including combustion, gasification, fuel cell and the Fischer-Tropsch (F-T) synthesis process. The species most likely to be present in the greatest amounts are those which are most stable under the conditions of interest, i.e., those having the lowest values of the free energy of formation. For the system containing carbon, hydrogen and oxygen in the temperature ranges of 298K to 1500K and a pressure of one atmosphere, the most stable species are carbon, carbon oxide, carbon dioxide, hydrogen, water and methane (1). For the F-T synthesis reaction, an iron catalyst is frequently employed. On contacting with the pretreating and/or synthesis gases, the iron or iron oxides can form an iron carbide, which is a catalyst for F-T synthesis. It is of interest to define the gas phase compositions where the iron carbide is thermodynamically favored during the course of catalyst activation and synthesis.

A convenient and informative method for the presentation of the iron carbide or iron oxide formation boundaries for the ternary CHO system is a set of triangular coordinates. The generality of the phase diagram becomes clear when it is recognized that C:H:O ratios of the system completely determine whether or not carbon, iron oxide and/or iron carbide will form for a given composition of gases. The usefulness of the phase diagram has been demonstrated by Manning and Reid (2) in their study of the iron-iron oxide system, Sacco and Reid (3) for the Bosch reaction system, and Sacco et al. (4) who studied the formation of carbon on iron.

This study considers the CHO gas phase compositions in equilibrium with iron and/or graphite (C) over the temperature range of interest for Fischer-Tropsch synthesis (200°C - 300°C) at pressures of 1 and 15 atmospheres. Different forms of iron oxide, i.e., Fe<sub>3</sub>O<sub>4</sub>, Fe<sub>2</sub>O<sub>3</sub> and FeO, and iron carbide, i.e., Fe<sub>3</sub>C, Fe<sub>2.2</sub>C and Fe<sub>2</sub>C, may be present during F-T synthesis. However, for simplicity and the availability of thermodynamic data, only Fe<sub>3</sub>O<sub>4</sub> and Fe<sub>3</sub>C are used to represent the iron compounds in these calculations.

In the F-T synthesis using an iron catalyst, Fe<sub>3</sub>C, Fe<sub>3</sub>O<sub>4</sub>, and C may form by reactions (1), (2) and (3), respectively:



The gas components are also subject to the water-gas shift reaction:



and methane is included as follows:



Also, hydrocarbons may be formed as, for example:



## RESULTS

Three pertinent equilibria, C/gases, Fe/Fe<sub>3</sub>O<sub>4</sub>/gases and Fe/Fe<sub>3</sub>C/gases were considered in the calculations. A modification of the method presented by Cairns and Tevebaugh was employed (1). Details of the calculation are given in Appendix A. Figures 1 to 3 are phase diagrams showing the Fe/Fe<sub>3</sub>O<sub>4</sub>/gases (□), Fe/Fe<sub>3</sub>C/gases (Δ) and C/gases (○) at 15 atm. total pressure and temperatures of 300, 200 and 270°C, respectively. These graphs are on a molar basis of C, O and H; thus, an equimolar mixture of H, C and O (0.33 moles of each) requires a syngas with H<sub>2</sub>/CO = 0.5. From these diagrams, one can delineate regions where Fe<sub>3</sub>C, Fe<sub>3</sub>O<sub>4</sub> and/or C would be expected to form when iron is in contact with different gas mixtures composed of hydrogen, oxygen and carbon at different temperatures. For example, for a gas mixture represented by a position which is located above the upper line (□) in Figures 1-3, Fe<sub>3</sub>C is the solid iron phase that is thermodynamically favored. Carbon could also be formed in this region if Fe<sub>3</sub>C catalyzed carbon formation at a rate comparable to F-T; i.e., reaction (3) would proceed to the right. The tie line for syngas of different H<sub>2</sub>/CO mole ratios is also included in Figure 1. This tie line clearly shows that in order to have iron present only as Fe<sub>3</sub>C, the H<sub>2</sub>/CO mole ratio of the syngas must be less than about 0.75 at 300°C.

After activation with CO, the iron should be present only as, or predominantly as, the carbide. Experimental data show the 90% or greater is present as iron carbide following a 24 hr activation period (5-7) (Figure 4). During the course of F-T synthesis, gas compositions change to produce a catalyst in which some Fe<sub>3</sub>C is converted to

Fe<sub>3</sub>O<sub>4</sub> (Figure 4, from ref. 5). Previous studies produced data to show that the formation of H<sub>2</sub>O during the F-T synthesis, i.e., reaction 6, is a major reason that Fe<sub>3</sub>C will change phase to Fe<sub>3</sub>O<sub>4</sub> (8). For a particular feedstock that defines the ratio of H<sub>2</sub>/CO, the composition of all gases can be calculated by using material balance equations for each conversion level of CO and H<sub>2</sub>.

Using equations 8 and 9 for the reaction stoichiometry, one can calculate the minimum time required to convert Fe<sub>3</sub>C to Fe<sub>3</sub>O<sub>4</sub> at particular reaction conditions.



or



This is done for typical F-T synthesis conditions (catalyst loading, 15 g Fe, T = 270°C, H<sub>2</sub>/CO = 0.67, flow rate = 3.1 L/hr./g.Fe, alpha = 0.7) where the H<sub>2</sub> and CO conversions are approximately 86 and 90%, respectively (9,10). Using these data, it is calculated that it would take approximately 4 hours to have sufficient reactants pass through the catalyst to convert Fe<sub>3</sub>C to an equilibrium mixture of Fe<sub>3</sub>C and Fe<sub>3</sub>O<sub>4</sub>. The actual time needed to convert iron carbides present following activation to a mixture of iron carbides/iron oxide has been determined experimentally for several catalysts (5-7) and is much longer than the minimum. The presence of promoters provides a complicating factor to the conversion and stability of the iron carbide phases. Thus, for a comparison with the calculation of the minimum time for the conversion of iron carbide to iron oxide, data for an iron catalyst that does not contain promoters are shown in Figure 4. It is emphasized that for the iron catalyst, data similar to that shown in Figure 4 have been obtained for several runs.

In addition to the data shown in Figure 4, data have also been reported for Mössbauer and XRD characterization of promoted and unpromoted iron catalysts withdrawn from the reactor at various times (5-7,9,10). While the extent of oxidation as well as the rate of oxidation of catalysts utilized in laboratory CSTRs and the LaPorte pilot plant may differ for these catalysts, the compositional changes that occur follow a trend that can be represented by the data in Figure 4.

The forms of the carbon present in the actual FTS catalyst is difficult to define. Certainly for operation in the high temperature range of FTS, free carbon may be deposited (11). In fact, these carbon deposits can be so large as to cause disintegration of the catalyst particle and its formation has reduced the iron catalyst particles to very fine "bug dust" (12).

Small iron carbide particles can be prepared using a laser pyrolysis technique (13) and these particles are surrounded by pyrolytic carbon with  $d = 0.35$  nm spacing between ordered layers. These carbon coated iron carbide particles have catalytic activity for FTS (10). Furthermore, the particles, depending upon preparative conditions, may initially be either  $\text{Fe}_7\text{C}_3$  or  $\text{Fe}_3\text{C}$  but, in either case, the carbide phase gradually converts to the oxide phase during use for FTS. Starting with large (100-1,000 nm) particles of  $\text{Fe}_2\text{O}_3$ , it has been shown that organized carbon layers form on the small particles of iron carbides that are formed during catalyst activation (14). The deposition of these organized pyrolytic carbon layers is not restricted to iron carbides. Nolan et al. (15) showed that organized carbon layers are present on both nickel and cobalt carbides. While the form of this organized carbon has not been conclusively defined, the use of graphite to represent this carbon seems reasonable.

A catalyst prepared by activation with CO at 270°C for 24 hours contains about twice the amount of carbon that is needed to form Fe<sub>5</sub>C<sub>2</sub> and is presumably present as organized "pyrolytic carbon" on the surface of the iron carbide particles. Similar results have been obtained using a 1-L CSTR, a 2" slurry bubble column reactor and the 22.5" i.d. slurry bubble column reactor at the LaPorte pilot plant (16). Following pretreatment in CO, the iron is essentially in the form of iron carbides.

### Comparison with Experimental Data

The compositional changes occurring with iron carbide catalysts during synthesis using conditions outlined in the manuscript have been documented in previous publications (5-7,9,10) and are representative of those shown in Figure 4.

F-T synthesis was effected at various CO conversion levels using a slurry reactor. Details of the experimental set-up, procedures and analytical methods are provided elsewhere (17,18). In one study (17), the molar ratio of syngas feed (H<sub>2</sub>/CO=0.67), pressure (175 psi), and temperature (270°C) were held constant while flow rates of syngas were varied between 9.5 and 75.6 NL/hr-gFe for CO (6.4 and 50.6 NL/hr for CO). The composition of the gas phase exiting the reactor for each conversion level is shown in Table 1. The hydrocarbons formed (i.e., C<sub>1</sub> to C<sub>35</sub>) during the reaction are reported in this table as an average value of C<sub>x</sub> H<sub>y</sub>. The mean carbon number of the hydrocarbon products is given by equation 10 (19):

$$x = 1 / (1 - \alpha) \quad (10)$$

where  $\alpha$  refers to chain growth probability. Since the  $\alpha$  value for this particular run is about 0.75 (17,18), the mean carbon number,  $x$ , is 4. The mean hydrogen number in the products can be calculated by:

$$y = \{ \sum [H/C]_i \cdot N_i / \sum N_i \} * x \quad (11)$$

where the mean carbon number  $x = 4$ ,  $i$  denotes hydrocarbon with carbon number equal to  $i$ , and  $N$  denote the molar fraction of each hydrocarbon. The data in Figure 5 indicate that at higher conversion levels, ( $X_{CO} = 0.69$  to  $0.86$ ),  $Fe_3C$  is the solid iron phase that is favored by thermodynamics. However, at lower conversion levels ( $X_{CO} = 0.23$  to  $0.46$ ) both  $Fe_3C$  and  $Fe_3O_4$  are thermodynamically favored. The data in Table 1 show that the concentration of  $H_2O$  increases to a maximum level and then decreases with increasing CO conversion. On the other hand, the concentration of  $CO_2$  increases with increasing CO conversion.

The data in Figure 6 indicate that the conversion of CO and  $H_2$  are approximately equal (i.e.,  $X_{CO} = X_{H_2} = 0.69$ ) at a total flow rate ( $CO+H_2$ ) of  $31.3$  NL/hr-gFe; this equal conversion is designated the equivalence point. At flow rates lower than the one that corresponds to the equivalence point, the conversion of  $H_2$  is greater than that of CO while the conversion of CO is greater than that of  $H_2$  above the equivalence point. This is due to the effect of WGS reaction since it consumes CO to generate  $H_2$ . For flow rates slower than the one corresponding to about the equivalence point,  $Fe_3C$  is the iron phase that is thermodynamically favored. However, for flow rates faster than the one corresponding to the equivalence point, both  $Fe_3C$  and  $Fe_3O_4$  are thermodynamically favored.

The solubility of the F-T gaseous reaction products,  $CO_2$  and  $H_2O$ , in the F-T reactor wax product is reported to be higher than CO and  $H_2$  by about a factor of ten; however, the solubilities of CO and  $H_2$  increase remarkably with temperature which is in contrast to the product gases where the solubilities decrease with increases of temperature (20). Knowing the partial pressure of gas phase compounds and assuming that vapor-liquid equilibrium occurs, the solubility of each gas can be

calculated using the data reported in references 17 and 20. The total amounts of the compounds ( $\text{CO}$ ,  $\text{H}_2\text{O}$ ,  $\text{CO}_2$ ,  $\text{CH}_4$ ) present in the reactor in both the gas and liquid phases can be calculated; these are shown in Figure 7. The data which represent both gas and liquid phase compounds are similar to the results in Figure 5, which represent only gas phase compounds.

## DISCUSSION

The thermodynamic data indicate that activation in  $\text{CO}$  or  $\text{H}_2/\text{CO}$  at compositions with a ratio of 0.7 or lower should produce a nearly pure iron carbide phase. The experimental data generated during a 24 hour activation in  $\text{CO}$  at  $270^\circ\text{C}$  (1 or 12 atm.) show nearly pure iron carbide is formed (Figures 4 and 8). However, during about 24 hours of  $\text{CO}$  activation in a CSTR at  $270^\circ\text{C}$ , about twice as much carbon is deposited as is required to produce an iron carbide. Thus, it is apparent that a form of free carbon is deposited as well during the 24 hour activation. It is a common feature to observe a carbon film on nanometer sized metal particles (13,15). Carbon films have also been observed for large-particle iron Fischer-Tropsch catalysts (14).

The reduction of the catalyst to iron is not expected in a static system at temperatures of  $300^\circ\text{C}$  and lower. In agreement with this expectation, only about 30% of the iron is present as  $\text{Fe}^0$  following 24 hour at  $270^\circ\text{C}$  in **flowing** hydrogen which continuously removes water (e.g., 5). Under reaction conditions, even at high conversion levels to produce high  $\text{H}_2/\text{CO}$  ratios, the presence of significant water (and  $\text{CO}_2$ ) will prohibit the reduction of the iron to  $\text{Fe}^0$ . In agreement with the calculations, metallic iron has not been observed in the catalyst samples withdrawn from the reactor during synthesis. Any metallic iron present following activation for 24 hours in  $\text{H}_2$  was converted to metal carbides within 2 hours exposure to synthesis gas (5).

Under conditions of synthesis with  $H_2/CO = 0.7$ , the calculated data based on the exit gas phase composition, and even including the excess CO and  $H_2O$  held in the liquid phase in the reactor, based upon measured solubilities, the iron catalyst should be present as the carbide phase (Figure 7). One of the reasons for the deviation of the experimental data from the equimolar C and O tie-line is that oxygen present in methanol, ethanol and other oxygenates have not been included in the calculation. However, a significant fraction of the iron in the catalyst is present as  $Fe_3O_4$  following long-term use in Fischer-Tropsch synthesis (5-7,9,10).

One possibility to account for the presence of both iron carbides and  $Fe_3O_4$  during Fischer-Tropsch synthesis is that errors in the thermodynamic data cause the actual region for the presence of both iron carbides and  $Fe_2O_3$  to extend to a higher carbon region than shown in Figures 1-3, 5 and 7.

A more likely possibility is inhomogeneity in the individual catalyst particles. In the interior of the individual porous particle and in the agglomeration of particles, the conversion of  $H_2$  and CO will produce  $CO_2$  and  $H_2O$  in addition to liquid hydrocarbons. The combination of reaction rates and product diffusion can combine to increase the concentration of  $H_2O$  and  $CO_2$  to levels that are higher than are present in the bulk gas phase. Thus, the individual catalyst particles could be present with a core of predominantly  $Fe_3O_4$  and with a surface layer of predominantly iron carbides coating the  $Fe_3O_4$  core.

This model provides an explanation for the lack of a direct correlation between bulk catalyst composition and catalytic activity/selectivity. In many of the early studies with the fused iron catalyst, it was necessary to reduce the mass to essentially pure metallic iron, and this was found to be the case for the C-73 catalyst provided by United

Catalyst Inc. (22). Results of the changes that occur when this catalyst is placed in the syngas is illustrated in Figure 9 (11). In a lecture in 1974, Emmett (21) summarized what happens to this type of catalyst during synthesis. He noted that, "The story of what happens to the iron is rather straightforward... Immediately one builds up a concentration of carbide - the carbide which is formed is  $\text{Fe}_2\text{C}$  and it builds up rather quickly to a considerable extent and the iron content of course very well drops, and then a somewhat slower reaction builds up  $\text{Fe}_3\text{O}_4$ . After a while the catalyst is largely  $\text{Fe}_3\text{O}_4$ ,  $\text{Fe}_2\text{C}$  and iron. The interesting thing is that it chugs along producing synthetic fuels at just about the same rate as it did initially. All of which reveals the fact that the surface composition is maybe distributed between iron,  $\text{Fe}_2\text{C}$  and  $\text{Fe}_3\text{O}_4$  and this is the thing that determines the activity of the catalyst and these various phases within the catalyst are simply bulk phases that form by-products that are not particularly concerned with the reaction...There is evidence that until these carbides build up very little hydrocarbons are synthesized. In other words, it is necessary to build up these carbides and oxides in order to block the center of the iron catalyst crystals so that the carbon that is formed momentarily on the surface is as some  $\text{Fe}_2\text{C}$  compound...So we have a catalyst that, when all is simply said and done, we simply have to conclude is a combination of iron, iron carbide and iron oxide and possibly the surface is made up of such a combination."

Various studies at the CAER have shown that a sample activated to produce a material that is predominantly  $\text{Fe}_3\text{O}_4$  has a much lower catalytic activity than one that is predominantly an iron carbide. Furthermore, the phases present are in a dynamic situation that depends upon the conversion levels of CO and  $\text{H}_2$ . Thus, at the surface of the catalyst particle, the CO appears to serve to imitate and to grow the hydrocarbon

chains as well to serve as a source of carbon to maintain at least the surface region of the catalyst particle as an iron carbide phase.

## **ACKNOWLEDGMENT**

This work was supported by U.S. DOE contract number DE-AC22-94PC94055 and the Commonwealth of Kentucky.

## REFERENCES

1. E. J. Cairns and A. D. Tevebaugh, *J. of Chem. and Eng. Data*, **9**, No. 3, 453 (1964).
2. M. P. Manning and R. C. Reid, *Ind. Eng. Chem. Proc. Des. Dev.*, **16**, No. 3, 358 (1977).
3. A. Sacco, Jr., and R. C. Reid, *AICHE J.*, **25**, No. 5, 839 (1979).
4. A. Sacco, Jr., P. Thacker, T. H. Chang, and A. T. S. Chiang, *J. Catal.*, **85**, 224 (1984).
5. C. S. Huang, B. G. Ganguly, G. P. Huffman, F. E. Huggins and B. H. Davis, *Fuel Sci. Tech. Int.*, **11**, 1289 (1993).
6. K. R. P. M. Rao, F. E. Huggins, V. Majahan, G. P. Huffman, V. U. S. Rao, B. L. Bhatt, D. B. Bukur, R. J. O'Brien and B. H. Davis, *Topics in Catal.*, **2**, 71 (1995).
7. K. R. P. Rao, F. E. Huggins, G. P. Huffman, R. J. Gormley, R. J. O'Brien and B. H. Davis, *Energy & Fuels*, **10**, 546 (1996).
8. J. A. Amelse, L. H. Schwartz and J. B. Butt, *J. Catal.*, **72**, 95 (1981).
9. R. J. O'Brien, L. Xu, D. R. Milburn, Y.-X. Li, K. J. Klabunde and B. H. Davis, *Topics in Catal.*, **2**, 1 (1995).
10. R. J. O'Brien, L. Xu, X. X. Bi, P. C. Eklund and B. H. Davis, Fischer-Tropsch synthesis and XRD characterization of an iron carbide catalyst synthesized by laser pyrolysis, in "The Chemistry of Transition Metal Carbides and Nitrides," (S. T. Oyama, Ed.), Chapman & Hall, London, pp 362-372, 1996.
11. M. E. Dry in "Catalysis: Science and Technology," (J. R. Anderson and M. Boudart, Eds.) Springer-Verlag, Berlin, 1981, Vol. 1, pp 159-255.
12. A. M. Squires, *Advan. Chem. Eng.*, **20**, 1-20 (1994).

13. R. Ochoa, X. X. Bi, A. M. Rao and P. C. Eklund in "Transition Metal Nitride and Carbide Nanoparticles," Blackie, Glasgow, United Kingdom, 1996, pp 489-510.
14. A. K. Datye, M. D. Shroff, M. S. Harrington, A. G. Sault and N. B. Jackson, "Natural Gas Conversion IV," (M. dePontes, et al., eds.) Elsevier, Amsterdam, 1997, pp 169-174.
15. P. E. Nolan, D. C. Lynch and A. H. Cutler, *Carbon*, **32**, 477 (1994).
16. B. L. Bhatt, "Liquid Phase Fischer-Tropsch (II). Demonstration in the LaPorte Alternative Fuels Development Unit," Final Technical Report, DOE Contract No. DE-AC22-91PC90018, September, 1995.
17. A. Raje, J. Inga and B. H. Davis, *Fuel*, **76**, 273 (1997).
18. A. Raje and B. H. Davis, *Catal. Today*, **36**, 335 (1997).
19. L. Caldwell and D. S. Van Vuuren, *Chem. Eng. Sci.*, **41**, 89 (1986).
20. H. Kölbel, P. Ackermann and Fr. Engelhardt, *Erdöl und Kohl*, **9**, 153 (1956).
21. P. H. Emmett, videotape of lecture at ORNL, 1974.
22. B. H. Davis, "Mechanism of Promotion of Fischer-Tropsch Catalysts," Final Report, DOE/PC/70029-T1, December, 1987.

## Appendix 1

### Method for Calculation

For a balanced chemical process, the change in thermodynamic property can be calculated by adding together the tabulated values of the property for the substances present in the final state minus the sum of the values of the properties for the substances in the initial state, each value being property multiplied by the appropriate stoichiometric coefficient. The procedures for calculating the equilibrium constant for a chemical reaction utilized obtains thermodynamic properties from reference (1). The equilibrium constants for each temperature were calculated from Gibbs free energy, obtained for the  $\Delta H^\circ$  and  $\Delta S^\circ$  fractions using the assumption of  $\Delta C_p^\circ$  is constant in the temperature range utilized.

### Equilibrium Calculation for Different Systems

The calculation for the system of C (graphite) and gases (CO, H<sub>2</sub>, CO<sub>2</sub>, H<sub>2</sub>O, CH<sub>4</sub>) equilibria, equations (3), (4) and (5) can be utilized. One material balance equation and three equilibrium constants collectively include all six species in equations (3), (4) and (5).

Material Balance		
Species	Moles at Start	Moles at Equilibrium
CO <sub>2</sub>	CO <sub>2,0</sub>	CO <sub>2,0</sub> - x + y
H <sub>2</sub>	H <sub>2,0</sub>	H <sub>2,0</sub> - x - 2z
C	0	y - z
CH <sub>4</sub>	0	z
H <sub>2</sub> O	0	x
CO	0	x - y

The variable x, y, and z can be calculated by substituting expressions from material balance into the equilibrium constant equations:

$$\frac{z}{(H_{2,0} - x - 2z)^2} = K_3 \quad (11)$$

$$\frac{(CO_{2,0} - x + y)}{(x - 2y)^2} = K_2 \quad (12)$$

$$\frac{x \cdot (x - 2y)}{(CO_{2,0} - x + y) (H_{2,0} - x - 2z)} = K_1 \quad (13)$$

with three equations and three variables, values for x, y and z can be obtained.

For the equilibria involving  $Fe_3O_4/Fe$  and gases ( $CO$ ,  $H_2$ ,  $CO_2$ ,  $H_2O$ ,  $CH_4$ ) equation (4)

and the following equations are applicable:



The appropriate compositions and equations are:

Material Balance		
Species	Initial	At Equilibrium
$CO_2$	0	$x - y - 4z$
$H_2$	$H_{2,0}$	$H_{2,0} - 2x - y$
$CO$	$CO_{1,0}$	$CO_{1,0} - 2x + y + 4z$
$Fe$	$Fe_{1,0}$	$Fe_{1,0} - 3z$
$H_2O$	0	y
$CH_4$	0	x
$Fe_3O_4$	0	z

$$K_1 = \frac{[y] [CO_{,0} - 2x+y+4z]}{[H_{2,0} - 2x-y] [x-y-4z]} \quad (21)$$

$$K_{2,3} = \frac{[x] [x-y-4z]}{[H_{2,0} - 2x-y]^2 [CO_{,0} - 2x+y+4z]^2} \quad (22)$$

$$k_4 = \frac{[CO_{,0} - 2x+y+4z]^4}{[x-y-4z]^4} \quad (23)$$

The above allows one to obtain values for x, [CO<sub>2</sub>] and [CH<sub>4</sub>].

Data #	H <sub>2</sub> (psi)	CO (psi)	H <sub>2</sub> O (psi)	CO <sub>2</sub> (psi)	C <sub>4</sub> H <sub>y</sub> (psi)	y	X,CO (%)	X,H <sub>2</sub> (%)	CO+H <sub>2</sub> (NL/hr)
1	25.4	26.7	4	78	55	8.63	0.86	0.8	15.9
2	32	43	6	72	36	8.52	0.78	0.76	21
3	39.4	60.1	8.49	61.1	20.154	8.48	0.685	0.692	31.3
4	50.3	89.5	10.7	32.6	5.27	8.44	0.46	0.54	63.1
5	54.8	102.4	10.3	18.8	3.14	8.43	0.32	0.45	91.6
6	59.24	107.3	9.23	11.8	1.82	8.36	0.23	0.37	126.2

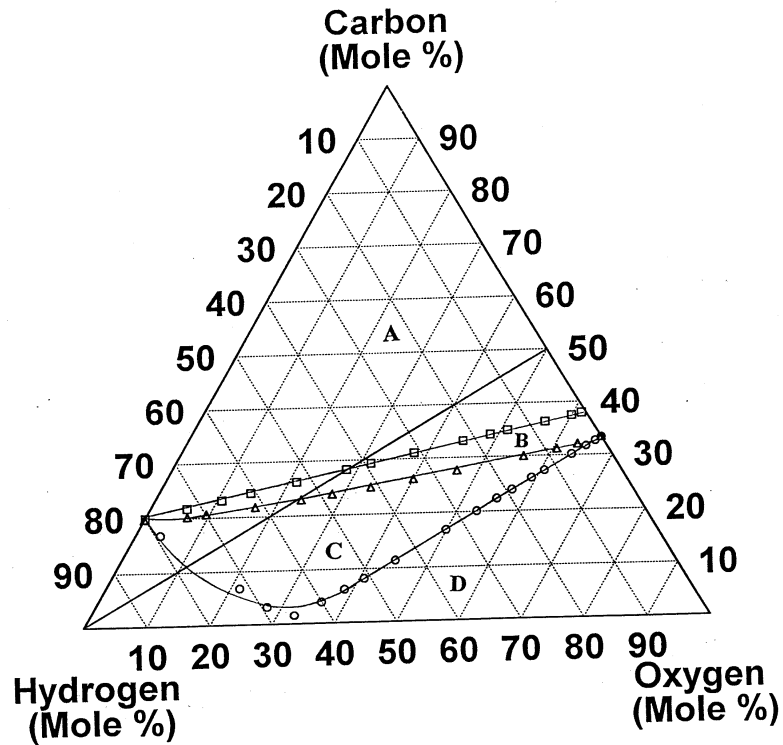


Figure 1. Ternary phase diagram for the solid phase(s) present for graphite/gases (○), Fe/Fe<sub>3</sub>O<sub>4</sub>/gases (□) and Fe/Fe<sub>3</sub>C/gases mixtures at equilibrium at 300°C and 15 atm. (Region A: Fe<sub>3</sub>C and C; Region B: Fe<sub>3</sub>O<sub>4</sub>, Fe<sub>3</sub>C and C; Region C: Fe<sub>3</sub>O<sub>4</sub> and C; Region D: Fe<sub>3</sub>O<sub>4</sub>; "—": tie line) (gases = H<sub>2</sub>O, CO, CO<sub>2</sub>, H<sub>2</sub> and CH<sub>4</sub>).

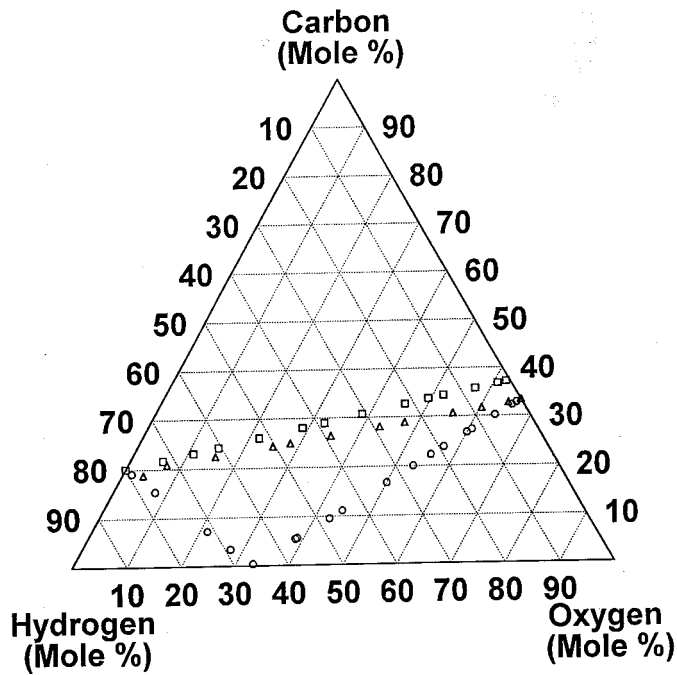


Figure 2. Ternary phase diagram for the solid phase(s) present for graphite/gases (○), Fe/Fe<sub>3</sub>O<sub>4</sub>/gases (□), Fe/Fe<sub>3</sub>C/gases mixtures (△) at equilibrium at 200°C and 15 atm. (gases = H<sub>2</sub>O, CO, CO<sub>2</sub>, H<sub>2</sub> and CH<sub>4</sub>).

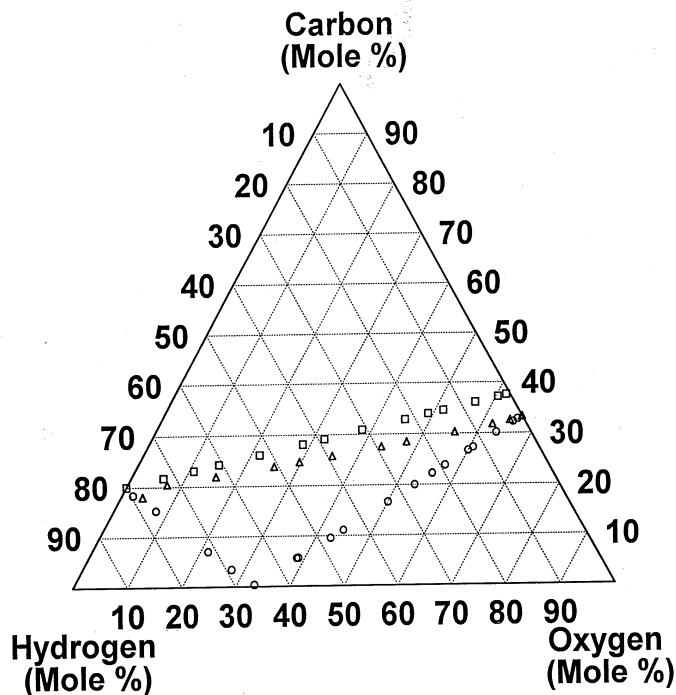


Figure 3. Ternary phase diagram for the solid phase(s) present for graphite/gases (○), Fe/Fe<sub>3</sub>O<sub>4</sub>/gases (□) and Fe/Fe<sub>3</sub>C/gases mixtures at equilibrium at 250°C and 15 atm. (gases = H<sub>2</sub>O, CO, CO<sub>2</sub>, H<sub>2</sub> and CH<sub>4</sub>).

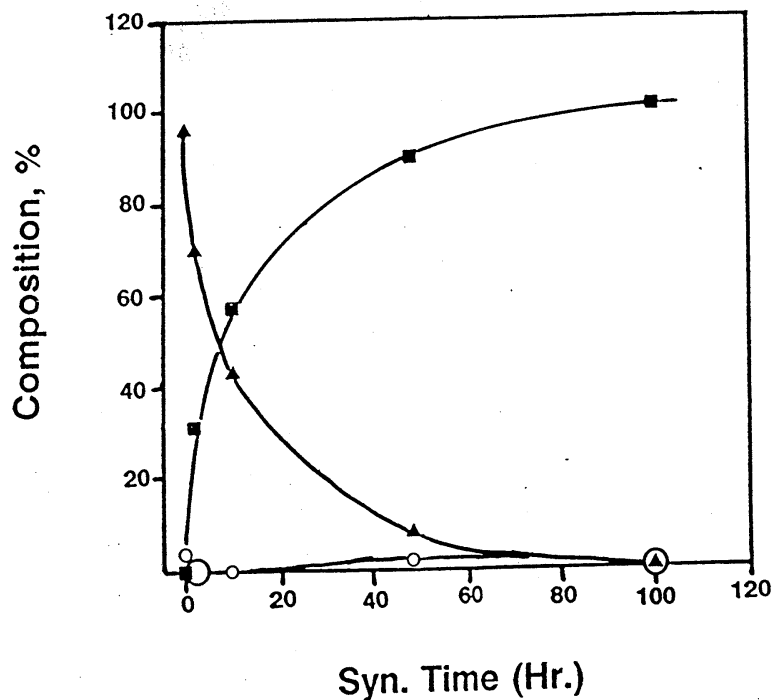


Figure 4. Change in composition of an activated iron catalyst during synthesis. Fe<sub>3</sub>O<sub>4</sub> (■), Fe<sub>2</sub>O<sub>3</sub> (○), and Fe carbides (▲) (high surface, 300 m<sup>2</sup>/g, 3.0 nm Fe<sub>2</sub>O<sub>3</sub>) (from ref. 5).

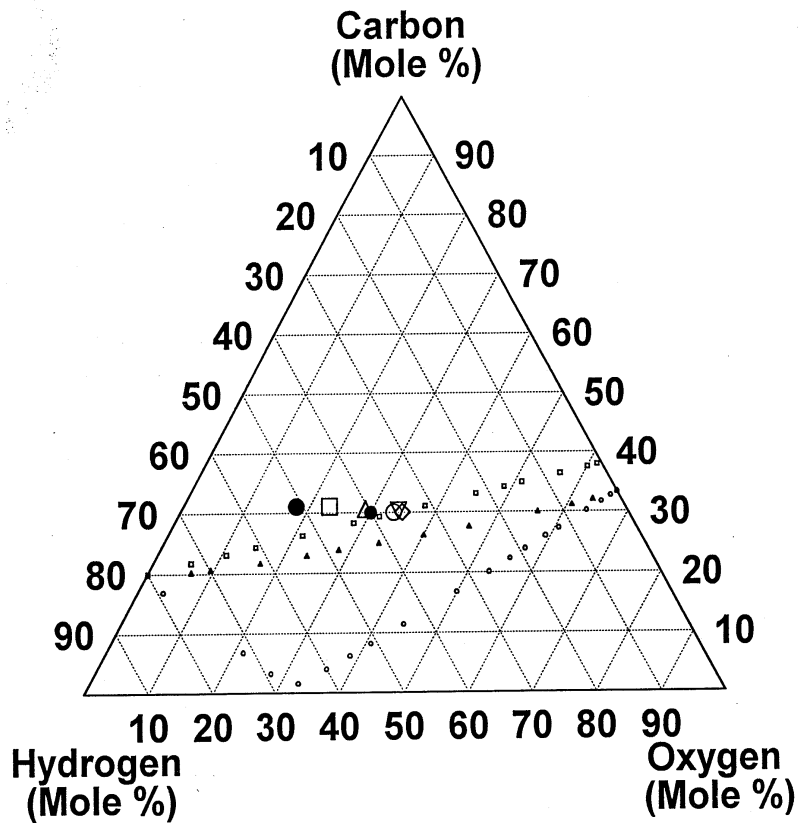


Figure 5. The gas phase composition during synthesis at various flow rates plotted on the ternary phase diagram of Figure 1. Data #1 in Table 1 (●), data #2 (□), data #3 (▲), data #4 (◇), data #5 (▽), data #6 (○) and feed composition of  $H_2/CO = 0.67$  (●).

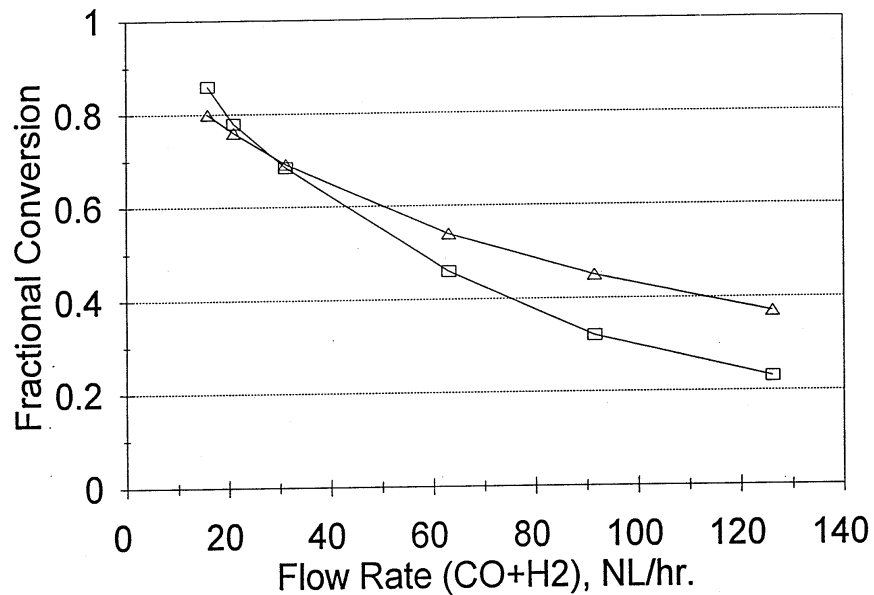


Figure 6. The variation of the conversion of  $H_2$  and  $CO$  with flow rate ( $H_2/CO = 0.7$ ,  $270^\circ C$  and  $170$  psig) (from ref. 9) (X,  $H_2$  (▲) and X,  $CO$  (□)).

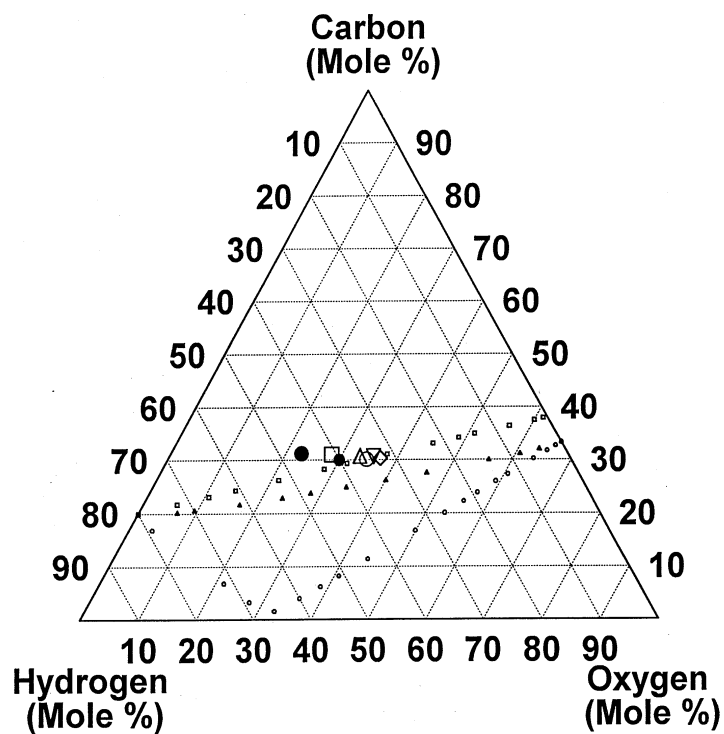


Figure 7. The gas phase composition during synthesis at various flow rates plotted on the ternary phase diagram of Figure 1 (both liquid and gaseous CO, H<sub>2</sub> and CO<sub>2</sub> and H<sub>2</sub>O are included in the calculation). Data #1 in Table 1 (●), data #2 (□), data #3 (Δ), data #4 (◇), data #5 (▽), data #6 (○) and feed composition of H<sub>2</sub>/CO = 0.67 (●).

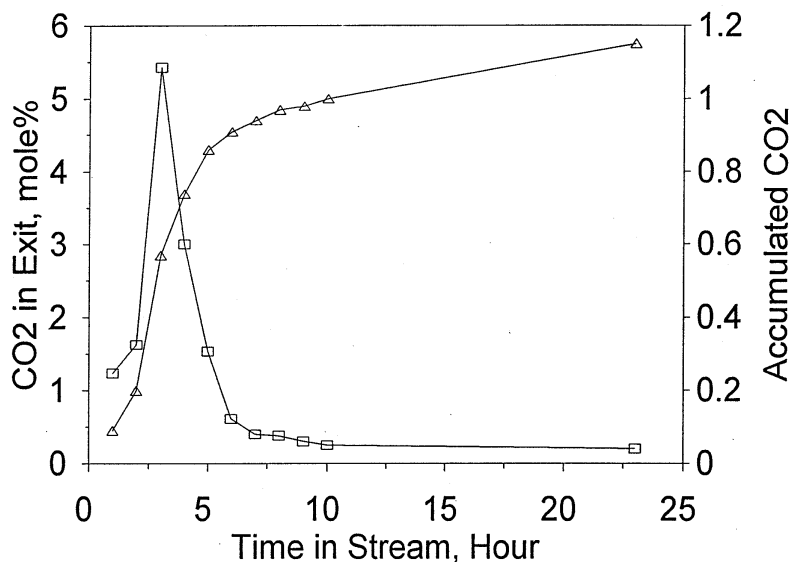


Figure 8. Rate of generation of CO<sub>2</sub> during activation of an iron catalyst at 270°C in a flow of CO in a 2 inch x 6 foot slurry bubble column reactor. CO<sub>2</sub> in exit (□) and accumulated CO<sub>2</sub> (Δ) represented by CO<sub>2</sub> formed/CO<sub>2</sub> formed to produce Fe<sub>3</sub>C.

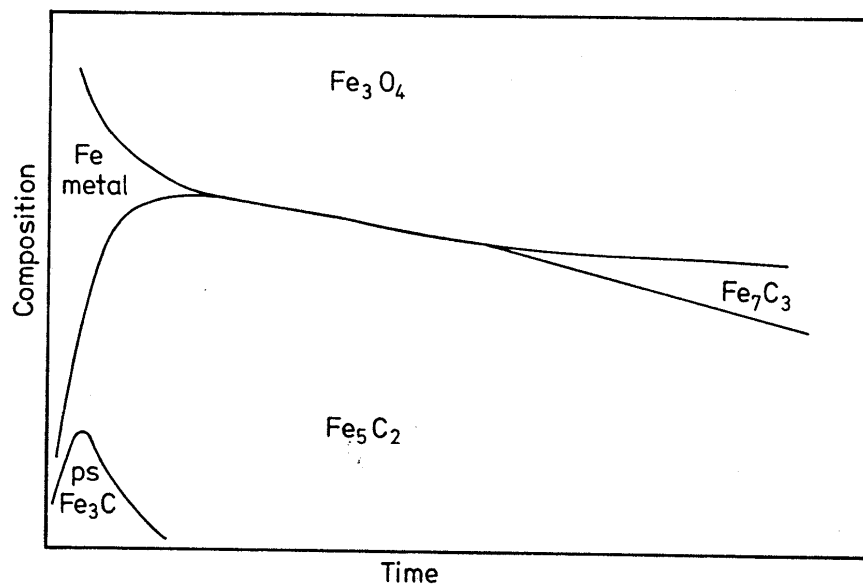


Figure 9. The change in the composition of iron catalysts during the FT reaction. The phases are those which are present according to X-ray diffraction analysis. At time zero the catalyst is 100% metallic Fe. The units are defined since the rates of the phase changes depend on alkali content. The figure is only intended to illustrate the trends (from ref. 11).